AtCCX3 Is an Arabidopsis Endomembrane H^+-Dependent K^+ Transporter[1][W][OA]

Jay Morris, Hui Tian, Sunghun Park, Coimbatore S. Sreevidya, John M. Ward, and Kendal D. Hirschi*

Vegetable and Fruit Improvement Center, Texas A&M University, College Station, Texas 77845 (J.M., S.P., K.D.H.); Plant Physiology Group, United States Department of Agriculture/Agriculture Research Service, Children's Nutrition Research Center, Department of Pediatrics, Baylor College of Medicine, Houston, Texas 77030 (J.M., K.D.H.); Department of Plant Biology, University of Minnesota, St. Paul, Minnesota 55108 (H.T., J.M.W.); and Department of Immunology, M.D. Anderson Cancer Center, Houston, Texas 77030 (C.S.S.)

The Arabidopsis (*Arabidopsis thaliana*) cation calcium exchangers (CCXs) were recently identified as a subfamily of cation transporters; however, no plant *CCX*s have been functionally characterized. Here, we show that Arabidopsis AtCCX3 (At3g14070) and AtCCX4 (At1g54115) can suppress yeast mutants defective in Na^+, K^+, and Mn^{2+} transport. We also report high-capacity uptake of $^{86}Rb^+$ in tonoplast-enriched vesicles from yeast expressing *AtCCX3*. Cation competition studies showed inhibition of $^{86}Rb^+$ uptake in *AtCCX3* cells by excess Na^+, K^+, and Mn^{2+}. Functional epitope-tagged AtCCX3 fusion proteins were localized to endomembranes in plants and yeast. In Arabidopsis, *AtCCX3* is primarily expressed in flowers, while *AtCCX4* is expressed throughout the plant. Quantitative polymerase chain reaction showed that expression of *AtCCX3* increased in plants treated with NaCl, KCl, and $MnCl_2$. Insertional mutant lines of *AtCCX3* and *AtCCX4* displayed no apparent growth defects; however, overexpression of *AtCCX3* caused increased Na^+ accumulation and increased $^{86}Rb^+$ transport. Uptake of $^{86}Rb^+$ increased in tonoplast-enriched membranes isolated from Arabidopsis lines expressing CCX3 driven by the cauliflower mosaic virus 35S promoter. Overexpression of *AtCCX3* in tobacco (*Nicotiana tabacum*) produced lesions in the leaves, stunted growth, and resulted in the accumulation of higher levels of numerous cations. In summary, these findings suggest that AtCCX3 is an endomembrane-localized H^+-dependent K^+ transporter with apparent Na^+ and Mn^{2+} transport properties distinct from those of previously characterized plant transporters.

The plant vacuole and other endomembrane compartments play an important role in the sequestration of various compounds (Marschner, 1995; Marty, 1999). Concentration gradients of Na^+, Ca^{2+}, Cd^{2+}, NO_3^-, and Mn^{2+} are established across these membranes by cation/H^+ exchange activities (Schumaker and Sze, 1985; Salt and Wagner, 1993; Barkla and Pantoja, 1996; Gonzalez et al., 1999). Several genes encoding these transport activities have been identified (Shigaki and Hirschi, 2006). However, the biological functions of many of the individual transporters remain for the most part undefined.

CCXs (for calcium cation exchangers) were previously identified as CAX (for cation exchanger) homologs. Recently CAX7 to CAX11 were reclassified as CCX1 to CCX5 due to higher homology to mammalian K^+-dependent Na^+/Ca^{2+} antiporters (Shigaki et al., 2006). CAXs are cation/H^+ antiporters that show high-capacity, low-affinity transport and have been characterized in a variety of plants (Blumwald and Poole, 1986; Kasai and Muto, 1990; Ettinger et al., 1999; Cheng et al., 2002; Luo et al., 2005). CAXs are energized by the pH gradient established by proton pumps such as H^+-ATPase or H^+-pyrophosphatase (Kamiya and Maeshima, 2004). Several plant CAXs have been characterized as vacuole-localized transporters, which function in H^+-coupled antiport of Ca^{2+}, Mg^{2+}, and Mn^{2+}, resulting in the accumulation of these cations in vacuoles (Hirschi, 1999; Pittman and Hirschi, 2001; Pittman et al., 2004a). CCXs have not been studied, and it would be interesting to compare and contrast their activities with those of CAXs and the less closely related $Na^+(K^+)/H^+$ exchangers of the NHX family.

CAX proteins have N-terminal regulatory domains (Pittman and Hirschi, 2001), and AtCAX1 and AtCAX2 were originally cloned as functional N-terminal deletions (lacking the negative regulatory domain; Hirschi et al., 1996). We refer to these forms as sCAX1 and sCAX2 (Shigaki and Hirschi, 2006). Tobacco (*Nicotiana tabacum*) plants expressing AtsCAX1 exhibit Ca^{2+}

[1] This work was supported by the U.S. Department of Agriculture/Agricultural Research Service (Cooperative Agreement no. 58–62650–6001), the National Science Foundation (grant nos. NSF 0344350 and NSF 020977), and the U.S. Department of Agriculture Cooperative State Research, Education, and Extension Service (grant no. 2005–34402–17121 to K.D.H.). The National Science Foundation (grant no. 0209792) funded work in the laboratory of J.M.W.

* Corresponding author; e-mail kendalh@bcm.tmc.edu.

The author responsible for distribution of materials integral to the findings presented in this article in accordance with the policy described in the Instructions for Authors (www.plantphysiol.org) is: Kendal D. Hirschi (kendalh@bcm.tmc.edu).

[W] The online version of this article contains Web-only data.

[OA] Open Access articles can be viewed online without a subscription.

www.plantphysiol.org/cgi/doi/10.1104/pp.108.118810

Downloaded from on January 17, 2018 - Published by www.plantphysiol.org
Copyright © 2008 American Society of Plant Biologists. All rights reserved.

deficiencies, leaf necrosis, tip burning, and hypersensitivity to ion imbalances, as well as increased tonoplast Ca^{2+}/H^+ transport activity (Hirschi, 1999). The N termini of CCXs lack homology with CAXs, and it is not known if the N terminus has a regulatory function.

Arabidopsis (*Arabidopsis thaliana*) *CCX*s are related to mammalian plasma membrane Na^+/Ca^{2+} exchangers (NCXs). The NCXs mediate the exchange of Na^+ for Ca^{2+} depending on the electrochemical gradients, and NCKXs (for Na^{2+}/Ca^{2+}-K^+ exchangers) transport K^+ and Ca^{2+} in exchange for Na^+ (Lytton, 2007). Interestingly, both NCX and NCKX exchangers can operate in a forward (Ca^{2+} exit) or reverse (Ca^{2+} entry) mode, which is mediated by the change in Na^+ gradients and the potential across the membrane (Cai and Lytton, 2004a). However, the extent to which CCX transporters from Arabidopsis transport Na^+ or K^+ has not been addressed.

To investigate the function of CCX transporters, we cloned *AtCCX3* and the closely related *AtCCX4*. We expressed the transporters in various yeast strains in order to compare and contrast their functions to those of AtCAX1 and AtNHX1 transporters. We monitored the expression and localization of AtCCX3 in yeast cells and in planta. Finally, we overexpressed *AtCCX3* in plants and examined ion uptake and plant growth. Collectively, these findings demonstrate that AtCCX3 is an endomembrane H^+-dependent K^+ transporter.

RESULTS

AtCCXs Show Homology to Mammalian NCKXs

A family of genes originally identified as members of plant *CAX*s (Maser et al., 2001) were recently found to have high similarity to mammalian *NCKX6* (a member of the CCX family) and weak similarity to *AtNHX1* (Supplemental Fig. S1A). Thus, these transporters were reclassified as AtCCXs (Shigaki and Hirschi, 2006). We hypothesized that these putative transporters might function in cation homeostasis. We prepared open reading frame (ORF) clones for AtCCX3 and AtCCX4 from Arabidopsis (Columbia ecotype) genomic DNA, since these genes were predicted to contain no introns. The cloned *AtCCX3* and *AtCCX4* open reading frames contained 1,935 and 1,938 nucleotides, which could encode 644 and 645 amino acids and produce putative proteins of 70.1 and 70.8 kD, respectively. AtCCX3 and AtCCX4 are 79.50% identical and 86.02% similar to one another. They share more identity (26.8% identical, 46.9% similar) with human (*Homo sapiens*) HsNCKX6 than with AtCAX1 (12.1% identical, 25.1% similar). In contrast to AtNHX1, a known plant Na^+ transporter, the *AtCCX*s have very little sequence homology (Supplemental Fig. S1A). Both AtCCX3 and AtCCX4 contain short N-terminal hydrophilic domains, which are not related to the AtCAX1 N-terminal autoinhibitory domain (Supplemental Fig. S1B). Comparisons of the AtCCX3, AtCCX4, and HsNKX6 proteins show a short (25 amino acids) N-terminal region, followed by five transmembrane domains separated from another seven transmembrane domains by a long hydrophilic region (75 amino acids for HsNCKX6 and 115 amino acids for AtCCX4). By contrast, AtCAX1 has a long N-terminal domain containing 65 amino acids and has two sets of four transmembrane domains separated by a shorter hydrophilic domain (35 amino acids). Also, AtCCX3, AtCCX4, and HsNCKX6 have very short (15 amino acids) C-terminal domains compared with AtCAX1, which has a longer C-terminal region (25 amino acids; Supplemental Fig. S1C). Phylogenetic analysis of AtCCX1 to AtCCX5, AtCAXs, and the human K^+-dependent Na^+/Ca^{2+} antiporter HsNCKX6 clearly indicates that CCXs are more closely related to the K^+-dependent Na^+/Ca^{2+} antiporter than to any of the *CAX*s (Supplemental Fig. S1A; Shigaki et al., 2006). Specifically, AtCCX3 and AtCCX4 share the characteristic α-repeats GNG(A/S)PD in α1 and (G/S)(N/D) SxGD in α2 with HsNCKX6 (Supplemental Fig. S1B; Cai and Lytton, 2004a, 2004b); these are highly conserved Ca^{2+} and Na^+ domains (Winkfein et al., 2003; Kang et al., 2005).

Expression of AtCCX3 and AtCCX4 in Yeast

AtCCX3 and AtCCX4 were cloned into the piHGpd vector (Nathan et al., 1999) for expression in yeast under the control of the GPD promoter. To test the possibility of a CCX N-terminal regulatory domain, we made a truncation in the AtCCX3 ORF (AtsCCX3). These plasmids were then introduced into the yeast strains AXT3 (*ena1*::HIS3::*ena4*, *nha1*::LEU2, *nhx1*::TRP1, *ura3*-1; Yokoi et al., 2002) and wx1 (*nhx1* mutant; Nass et al., 1997) with defects in vacuolar Na^+/K^+ transport. *AtCCX3* and *AtCCX4* expression did not alter growth of the yeast in Arg phosphate (AP) medium (Fig. 1A) compared with vector controls. Also, expression of *AtsCCX3* or *AtNHX1* did not affect the growth of the yeast strain (Fig. 1A). AtCCX3 and AtCCX4 suppressed the Na^+ and K^+ sensitivity of these yeast strains (AXT3 and wx1) deficient in vacuolar Na^+/H^+ transport (Fig. 1, B and C); however, AtsCCX3 did not suppress the Na^+ and K^+ sensitivity in these strains. We also tested both the hemagglutinin (HA)-AtCCX3 and AtCCX3-GFP tagged proteins, and they both showed similar phenotypes to the native AtCCX3 (data not shown). Yeast cells expressing all of the *AtCCX3* and *AtCCX4* variants were unable to suppress the Ca^{2+} sensitivity of yeast strains deficient in vacuolar Ca^{2+} transport (data not shown). Yeast cells expressing AtCAXs all show increased Ca^{2+} transport when truncated in their N-terminal domain (Hirschi, 1999; Shigaki et al., 2001, 2003; Pittman et al., 2004b). A lack of N-terminal regulation, the ability to suppress Na^+-sensitive phenotypes, and the inability to suppress Ca^{2+}-sensitive phenotypes in yeast suggests functions for AtCCX3 and AtCCX4 that differ from those of CAXs.

Downloaded from on January 17, 2018 - Published by www.plantphysiol.org
Copyright © 2008 American Society of Plant Biologists. All rights reserved.

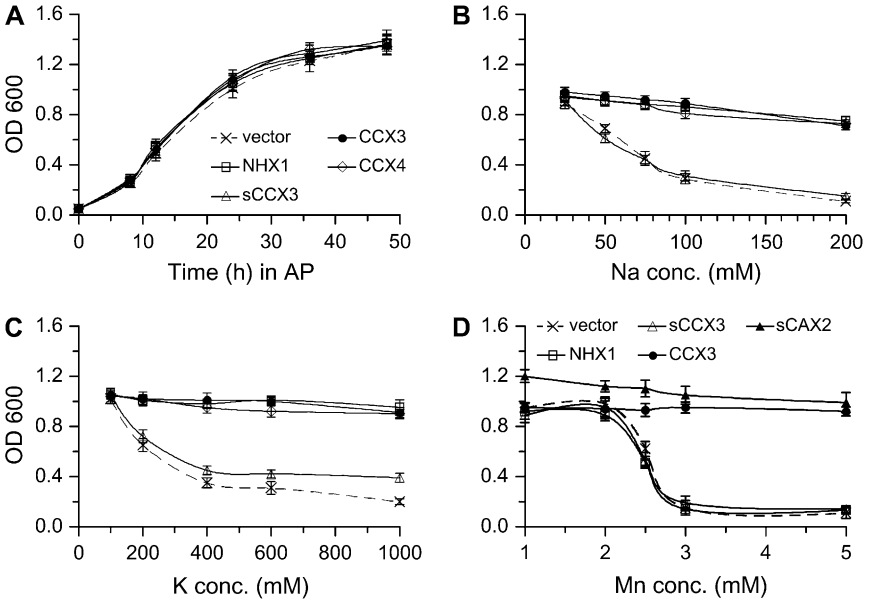

Figure 1. Growth of *AtCCX3*-expressing yeast strains in AP and YPD media with different cation concentrations. A, Growth of yeast strain wx1 (*nhx1*) transformed with vector (p2UGpd; crosses), *AtNHX1* (squares), AtsCCX3 (triangles), *AtCCX3* (black circles), or *AtCCX4* (diamonds) in AP over time. B, OD at 48 h for yeast strain AXT3 (*ena1*::HIS3::*ena4*, *nha1*::LEU2, *nhx1*::TRP1, *ura3-1*) grown in AP with different concentrations of NaCl + 1 mM KCl. C, OD at 48 h for yeast strain wx1 (*nhx1*) transformed with vector (p2UGpd), *AtNHX1*, *AtCCX3*, AtsCCX3, or *AtCCX4* in AP with various concentrations of KCl. D, OD at 48 h for yeast strains (Δsmf1 + Δsmf2) transformed with vector (p2UGpd; crosses), *AtNHX1* (squares), AtsCCX3 (triangles), *AtCCX3* (black circles), or AtsCAX2(black triangles) in AP over time grown in YPD with different concentrations of $MnCl_2$. Yeast strains expressing the different plasmids ($n = 8$) were serial diluted 125-fold, and 10 μL was placed into 190 μL of liquid selection medium containing NaCl, KCl, or $MnCl_2$.

We also tested the possibility that AtCCX3 and AtCCX4 transport other metals, thus making the host yeast cells tolerant or hypersensitive to these metals. Expression of *AtCCX3* in an Mg^{2+}-requiring strain (CM66) did not suppress the ion sensitivity of these strains (MacDiarmid and Gardner, 1998). *AtCCX3*-expressing cells were also tested with a range of metals, such as Al^{3+}, Cd^{2+}, Cu^{2+}, Ni^{2+}, and Zn^{2+}, in various mutant yeast strains (K661, K667; Salt and Wagner, 1993; Cunningham and Fink, 1996; Liu et al., 1997; Tuttle et al., 2003). In each case, *AtCCX3* cells were indistinguishable from vector controls in our assay conditions. However, expression of *AtCCX3* could suppress Mn^{2+} growth sensitivity in a yeast strain defective in both plasma and vacuolar membrane Mn^{2+} transport (smf1 + smf2; Supek et al., 1996; Cohen et al., 2000; Luk and Culotta, 2001; Fig. 1D). AtsCCX3 was unable to suppress the Mn^{2+} growth sensitivity, suggesting that truncating AtCCX3 does not activate a function that is different from that of the CAXs, where N-terminal truncations enhance function (Hirschi et al., 1996; Hirschi, 1999; Pittman and Hirschi, 2001; Pittman et al., 2002a, 2002b). This suppression of Mn^{2+} sensitivity phenocopied AtsCAX2 expression, a known vacuolar Mn^{2+} transporter (Fig. 1D; Pittman et al., 2004b). However, this is the only phenotype that overlaps with CAX transporters, and the other transport properties firmly establish distinct non-CAX functions for AtCCX3.

Transport Properties of AtCCX3 in Yeast

In order to determine whether AtCCX3 mediated K^+ transport, we measured $^{86}Rb^+$ uptake as a tracer for K^+ into yeast cells and yeast microsomal membranes (Venema et al., 2002; Pittman et al., 2004a, 2004b). In *wx1* yeast, only cells expressing *AtCCX3* or *AtNHX1* showed higher $^{86}Rb^+$ uptake at high K^+ concentrations (20 mM; data not shown) relative to vector controls. At low external K^+ (0.02 mM) concentrations, $^{86}Rb^+$ uptake by cells expressing *AtCCX3* and *AtNHX1* was similar to that of vector controls (data not shown). This suggests that AtCCX3 can facilitate K^+ uptake with low affinity in yeast, although it is unclear whether K^+ uptake is mediated directly or indirectly by CCX3.

Transport assays were performed using vacuole membrane-enriched vesicles from yeast. Membranes isolated from *wx1* cells expressing *AtCCX3* or *AtNHX1* showed increased $^{86}Rb^+$ uptake at 50 mM K^+ concentrations (Fig. 2A) than that of wx1 with vector only. At low external K^+ (0.5 mM) concentrations, $^{86}Rb^+$ uptake by cells expressing *AtCCX3* and *AtNHX1* was similar to that of vector controls (data not shown). As shown before, uptake of $^{86}Rb^+$ by AtNHX1 was inhibited by

Downloaded from on January 17, 2018 - Published by www.plantphysiol.org
Copyright © 2008 American Society of Plant Biologists. All rights reserved.

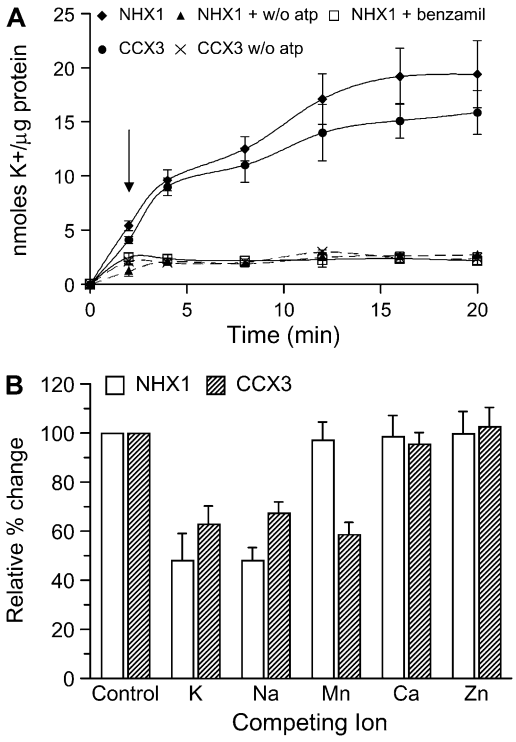

Figure 2. AtCCX3 or AtNHX1 mediates cation uptake into yeast vacuolar vesicles. A, K^+ ($^{86}Rb^+$) uptake into yeast vacuolar vesicles. Benzamil (10 μM; arrow) was added 2 min after addition of $^{86}Rb^+$. K^+ concentration was 50 mM; $n = 6$. Values shown are means ± SE. B, Effect of various cation chlorides (300 μM) on K^+ ($^{86}Rb^+$) uptake at 8 min. Values shown are means ± SE from six replicate measurements.

benzamil (Venema et al., 2003). However, treatment of *AtCCX3*-expressing yeast cells with benzamil to measure $^{86}Rb^+$ uptake inhibition was inconclusive (data not shown). Uptake of $^{86}Rb^+$ from both AtNHX1 and AtCCX3 required $MgCl_2$, as the removal of $MgCl_2$ resulted in a reduction in $^{86}Rb^+$ uptake (Fig. 2A). These results support the idea that Mg^{2+} is required to activate the vacuole-type H^+-ATPase to generate a pH gradient across the vesicle. Thus, in yeast, AtCCX3 appears to behave as a low-affinity K^+/proton exchanger in a manner similar to AtNHX1.

These phenotypes suggest that AtCCX3 has a role in K^+ transport, but the suppression of the Δsmf1, Δsmf2 Mn^{2+}-sensitive yeast strain also suggests that AtCCX3 functions in Mn^{2+} transport (Cohen et al., 2000). To further investigate the yeast phenotypes, $^{86}Rb^+$ uptake into vesicles was measured in the presence of excess nonradioactive KCl, NaCl, $MnCl_2$, $CaCl_2$, and $ZnCl_2$. Excess (300 μM) KCl and NaCl reduced $^{86}Rb^+$ uptake mediated by AtNHX1 and AtCCX3 by 50% and 40%, respectively (Fig. 2B), but no decrease in uptake was measured in the presence of excess $CaCl_2$ or $ZnCl_2$. Intriguingly, $MnCl_2$ only reduced AtCCX3-mediated uptake of $^{86}Rb^+$ but not that of AtNHX1 (Fig. 2B). Taken together, these results suggest that AtCCX3 mediates H^+-dependent uptake of K^+ and Na^+, similar to NHX1, yet is distinct in its cation specificity to a divalent cation, such as Mn^{2+}.

Metal Measurements in Yeast Expressing *AtCCX3* and *AtNHX1*

We tested the alkali cation content in mutant alone or in yeast strains expressing *AtCCX3* and *AtNHX1* after cells were exposed to 100 mM NaCl or KCl. Yeast cells expressing *AtCCX3* and *AtNHX1* showed a 25% increase in Na^+ and a 50% increase in K^+ content, compared with yeast cells expressing only the vector (Fig. 3). Thus, CCX3 promotes Na^+ or K^+ uptake similar to NHX1. In a preliminary experiment of wild-type W303-1A yeast cells expressing *AtCCX3*, the Mn^{2+} content was 85% higher compared with that in cells expressing only vector. Thus, *AtCCX3* expressed in yeast cells could play a role in Na^+, K^+, and Mn^{2+} homeostasis.

Localization of AtCCX3 in Yeast and Plants

An N-terminal HA-tagged AtCCX3 construct conferred resistance to high Na^+ and K^+ stress in wx1 (data not shown). We utilized this construct to identify the cellular location of AtCCX3. As shown in Figure 4A, western-blot analysis of yeast membranes fractionated on Suc gradients showed that AtCCX3 colocalized with vacuolar membranes. The distribution of HA-AtCCX3 corresponded with the yeast vacuolar membrane marker alkaline phosphatase but not with the plasma membrane marker Pma1p. As further confir-

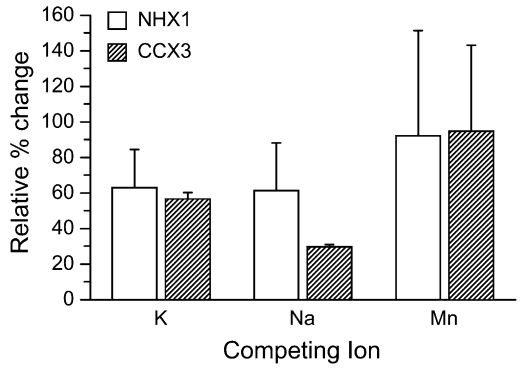

Figure 3. K^+ and Na^+ contents in *wx1* yeast expressing AtCCX3. Relative percentage change in K^+ and Na^+ between yeast wx1 vector control and wx1 transformed with *AtNHX1* or *AtCCX3* grown in medium containing 100 mM NaCl. ICP analysis was done on filtered whole yeast cells. Values shown are mean percentage differences ± SE from four replicate measurements. Calculated SE is for the relative percentage difference of the means. SE was calculated as (mean CCX3/mean vector) × (square root of z) × 100 (http://www.census.gov/acs/www/Downloads/ACS/PercChg.pdf). Concentrations of K^+ ions in wx1 yeast cells expressing various constructs were 25,107 $\mu g\ g^{-1}$ vector, 35,643 $\mu g\ g^{-1}$ *AtNHX1*, and 40,275 $\mu g\ g^{-1}$ *AtCCX3*; concentrations of Na^+ ions were 4,477 $\mu g\ g^{-1}$ vector, 6,047 $\mu g\ g^{-1}$ *AtNHX1*, and 5,873 $\mu g\ g^{-1}$ *AtCCX3*.

Downloaded from on January 17, 2018 - Published by www.plantphysiol.org
Copyright © 2008 American Society of Plant Biologists. All rights reserved.

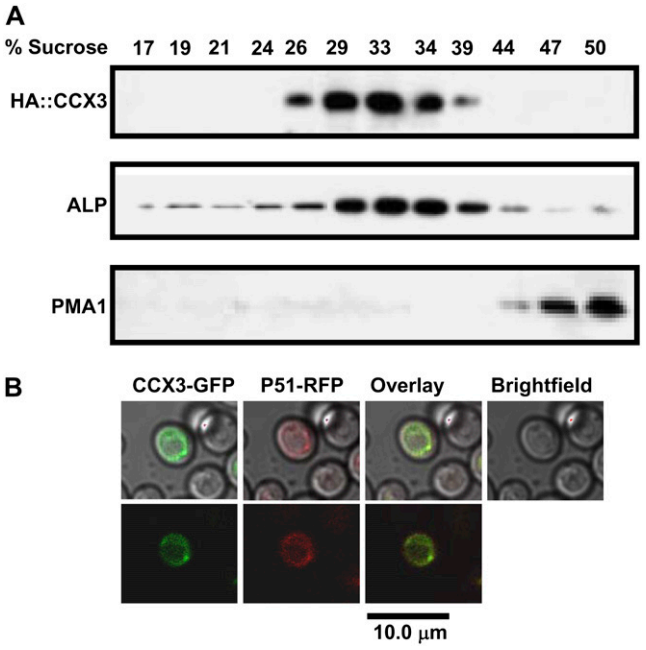

Figure 4. Subcellular localization of AtCCX3 in yeast. A, Subcellular localization of epitope-tagged HA-AtCCX3 to the vacuole membrane. Yeast membranes were fractionated on 10% to 50% (w/w) Suc gradients, and equal amounts of protein (15 mg) were separated by SDS-PAGE, blotted, and subjected to western-blot analysis using antibodies against HA, the vacuolar membrane marker alkaline phosphatase (ALP), and the plasma membrane H^+-ATPase (PMA1). B, Subcellular localization of CCX3-GFP. GFP was fused to the C terminus of full-length AtCCX3 and coexpressed with the yeast vacuolar membrane protein P51. The fusion protein and vacuolar marker were observed by confocal microscopy. The green channel (excitation at 488 nm, emission at 522 nm, and barrier filter at 522–535 nm) and red channel (excitation at 480 nm, emission at 530 nm with a fluorescent long-pass filter) images were captured with Fluoview software (Olympus America).

mation of yeast endomembrane localization, the AtCCX3-GFP expressed in yeast also appeared to reside on intracellular membranes, as the signal overlapped with vacuolar protein P51 fused to red fluorescent protein (Fig. 4B; Carter et al., 2004). These results suggest that AtCCX3 functions as an endomembrane cation transporter in yeast.

To investigate the subcellular localization of AtCAX3 in plants, microsomal membranes from transgenic lines harboring the AtCCX3-GFP fusion protein were fractionated. Centrifugation through a linear Suc gradient was first used to compare the distribution of the epitope-tagged transporter in transgenic Arabidopsis (Fig. 5A) with that of markers for the tonoplast, plasma membrane, and endoplasmic reticulum lumen. As shown in Figure 5A, the tagged proteins were located in fractions of 26% to 37% Suc. The AtCCX3-GFP protein was associated with fractions enriched in endomembranes, as indicated by the sedimentation profiles, which overlapped with a vacuole-type H^+-ATPase (V-ATPase subunit B; Ward et al., 1992) but not with an endoplasmic reticulum (BiP; Cheng et al., 2002) or the plasma membrane (AHA3; Pardo and Serrano, 1989) protein. To provide further confirmation for the localization in plants, we examined the transient expression of AtCCX3-GFP in onion (*Allium cepa*) cells (Sivitz et al., 2007). Fluorescence associated with 35S::GFP alone was localized to both the cytosol and the nucleus. In contrast, fluorescence was consistent with cytoplasmic vesicles and the vacuolar membrane, but some localization to the plasma membrane cannot be excluded in plant cells expressing 35S::AtCCX3-GFP (Fig. 5B).

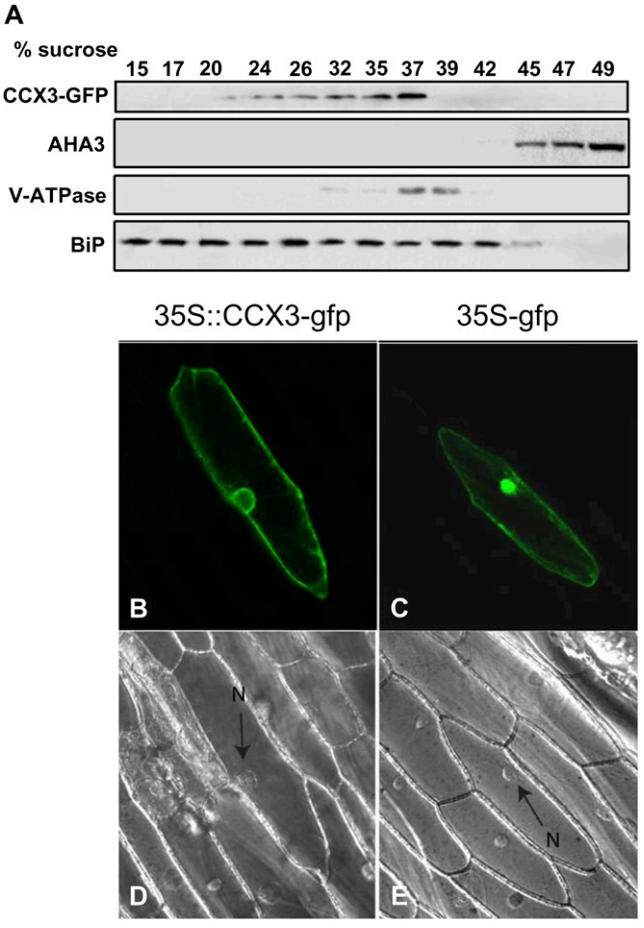

Figure 5. AtCCX3 localization in plants. A, Localization of epitope-tagged CCX3-GFP to the tonoplast. Arabidopsis microsomal membranes were fractionated on 10% to 50% (w/w) Suc gradients. Aliquots were collected and equal amounts of protein (10 mg) were separated by SDS-PAGE, blotted, and subjected to western-blot analysis using antibodies against GFP and plant membrane markers: the vacuolar ATPase subunit B, the plasma membrane H^+-ATPase (AHA3), and the endoplasmic reticulum protein (BiP; StressGen Biotechnologies). B and C, Projection confocal images of onion epidermis transiently expressing 35S::CCX3-GFP (B) or 35S::GFP (C). D and E, Differential interference contrast images of onion epidermis (D corresponds to B and E corresponds to C). The arrows indicate the position of the nucleus in D and E.

Downloaded from on January 17, 2018 - Published by www.plantphysiol.org
Copyright © 2008 American Society of Plant Biologists. All rights reserved.

Expression of *AtCCX3* and *AtCCX4* in Arabidopsis

Analysis of publicly available Arabidopsis microarray data indicates that *AtCCX3* is expressed at very low levels and predominantly in flowers and pollen grains (Bock et al., 2006; https://www.genevestigator.ethz.ch). This low level of expression made the use of northern blot and GUS promoter::reporter analysis difficult (data not shown). In order to more precisely monitor expression, we conducted reverse transcription (RT)-PCR and detected the expression of *AtCCX3* primarily in flowers, roots, and stems of wild-type Arabidopsis (Fig. 6A). *AtCCX4* appears to be expressed in pollen and throughout the plant and at levels substantially higher than *AtCCX3* (Bock et al., 2006; https://www.genevestigator.ethz.ch).

The ability of AtCCX3 to suppress a yeast mutant sensitive to Na^+ and K^+ and the increased sensitivity of wild-type yeast to Mn^{2+} prompted us to examine whether these or other cations could induce *AtCCX3* expression in Arabidopsis roots, leaves, and flowers. Expression of *AtCCX3* increased 2- to 3-fold in response to exogenous Na^+ and K^+, and by 0.5-fold compared with Mn^{2+}, in both roots and flowers (Fig. 6B). We then directly compared the changes in *AtCCX3* expression with those of *AtNHX1* under salt stress conditions. An increase in *AtNHX1* in response to Na^+ has been reported previously (Yokoi et al., 2002). Although *AtCCX3* is expressed at much lower levels than *AtNHX1*, expression of both genes was induced by Na^+ treatment in roots, leaves, and flowers (Fig. 6C). However, the basal level of *AtNHX1* expression was much higher than that of *AtCCX3*.

Analysis of T-DNA Insertional Mutants of *AtCCX3* and *AtCCX4*

To investigate the physiological function of AtCCX3 and AtCCX4 in Arabidopsis, we obtained two independent lines containing T-DNA insertions inside each open reading frame (Supplemental Fig. S2D). Homozygous lines were isolated by screening for the presence of the T-DNA insert and lack of native *AtCCX*. We isolated two different mutant alleles for *AtCCX3*, termed *atccx3-1* and *atccx3-2*, and two alleles for *AtCCX4*, termed *atccx4-1* and *atccx4-2*. RT-PCR analysis of the four different alleles showed no expression of *AtCCX3* or *AtCCX4* in the respective mutants (Supplemental Fig. S2, B and C). Pollen viability, pollen tube growth, and seed set were not altered in these mutants (data not shown), nor were there any other discernible growth abnormalities.

Ectopic Expression of *AtCCX3*

To further test the function of AtCCX3 in Arabidopsis, AtsCCX3 and *AtCCX3* were expressed using the cauliflower mosaic virus 35S promoter. Despite increased expression of *AtCCX3* RNA in the Arabidopsis lines, no visible changes in plant growth or development were detected (Supplemental Fig. S2A; J. Morris, unpublished data). However, lack of an *AtCCX3*-specific antibody prevented actual quantification of alterations of AtCCX3 protein amounts.

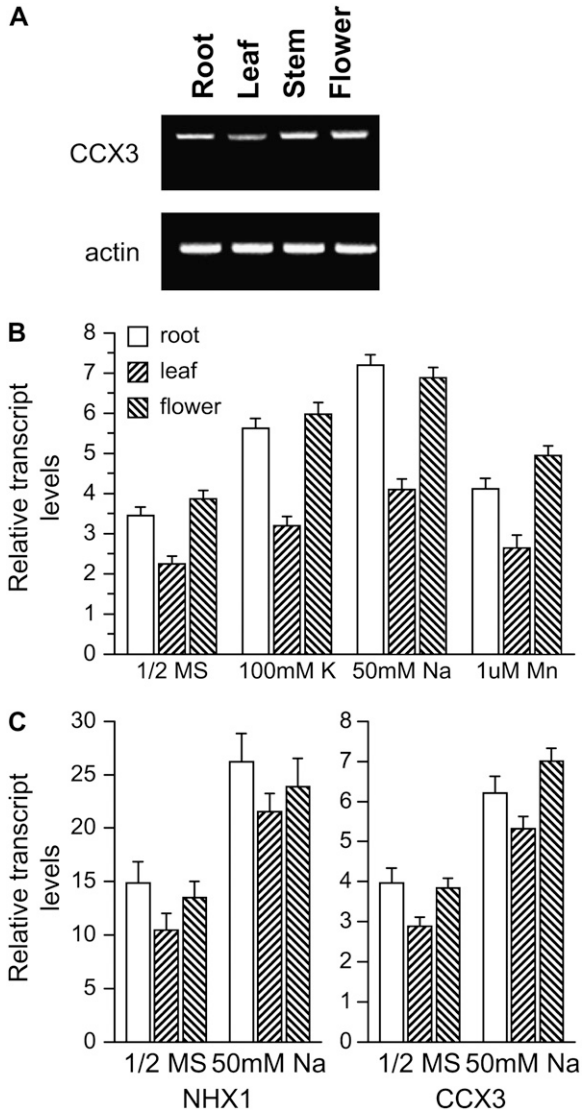

Figure 6. Expression of *AtCCX3* in Arabidopsis. A, RT-PCR shows *AtCCX3* expression in Columbia wild-type tissues. B, The relative expression levels of AtCCX3 in roots, leaves, and flowers in response to various cation treatments were normalized to expression of the *18S* subunit. The results were obtained from two independent RNA pools for each tissue and treatment combination analyzed. C, Comparison of *AtCCX3* expression with *AtNHX1* in roots, leaves, and flowers in response to 50 mM NaCl. Expression levels of *AtCCX3* and *AtNHX1* were normalized to expression of the *18S* subunit. Values shown are means ± SE from four replicate measurements.

35S::*AtCCX3* Arabidopsis plants treated with exogenous NaCl accumulated 35% more Na^+ compared with controls (26,490 ± 370 $\mu g\ g^{-1}$ dry weight for 35S::*AtCCX3*, 17,305 ± 2,145 $\mu g\ g^{-1}$ dry weight for controls). In contrast, when grown under normal conditions, there was only a modest Na^+ accumulation in

Downloaded from on January 17, 2018 - Published by www.plantphysiol.org
Copyright © 2008 American Society of Plant Biologists. All rights reserved.

35S::*AtCCX3* lines (6,044 ± 55 μg g^{-1} for 35S::*AtCCX3*, 5,772 ± 73 μg g^{-1} for controls).

To determine the in planta K^+ transport properties of AtCCX3, direct ^{86}Rb uptake assays into whole plants and vacuole-enriched vesicles isolated from Arabidopsis roots were assayed (Pittman et al., 2004a). Given the difficulty of inferring function from whole plant uptake assays, we isolated tonoplast-enriched vesicles to better understand the function of AtCCX3 in planta. Vesicles from 35S::*AtCCX3* and *AtNHX1* plants both showed higher ^{86}Rb uptake at high K^+ concentrations (50 mM; Fig. 7A) and no uptake at low external K^+ concentration (0.05 mM; data not shown). Similar to the yeast membranes, uptake of ^{86}Rb in membranes isolated from *AtNHX1* plants was inhibited by benzamil (Fig. 7A; Venema et al., 2002). As in our yeast assay, benzamil showed less inhibition on ^{86}Rb uptake into membranes from 35S::*AtCCX3* plants. Reduced uptake of ^{86}Rb in both *AtNHX1*- and 35S::*AtCCX3*-expressing plants was found when the H^+ gradient was disrupted by removing $MgCl_2$ from the reaction mixtures. Like our yeast assays, these plant membrane uptake values suggest that AtCCX3 is an H^+-driven Na^+, K^+, and Mn^{2+} exchanger.

We also tested the inhibition of ^{86}Rb uptake by competition with excess (300 μM) nonlabeled cation chlorides. Similar to our results in yeast, excess KCl and NaCl reduced ^{86}Rb uptake, while $CaCl_2$ and $ZnCl_2$ had no effect on ^{86}Rb uptake into membranes isolated from cells expressing *AtNHX1* and *AtCCX3* (Fig. 7B). However, excess $MnCl_2$ reduced the uptake of ^{86}Rb by 57% in membranes from 35S::*AtCCX3*-expressing membranes but showed no inhibition of ^{86}Rb uptake in *AtNHX1*-expressing membranes (Fig. 7B). These transport measurements again suggest that AtCCX3 has a role in Na^+, K^+, and Mn^{2+} homeostasis in planta.

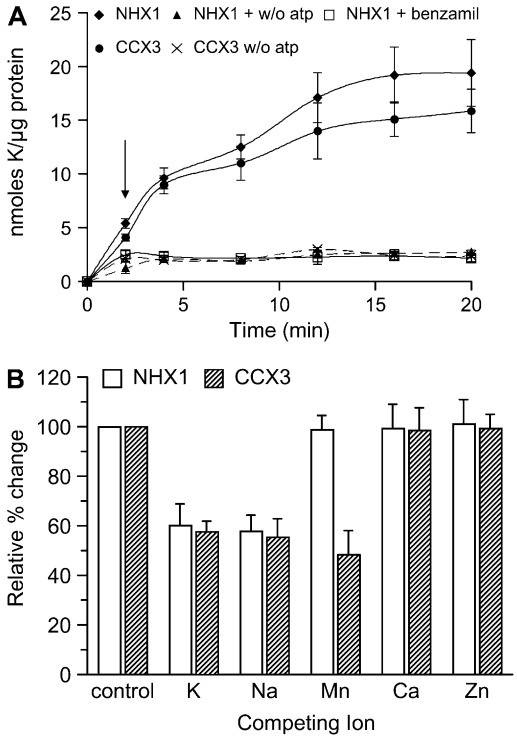

Figure 7. Cation uptake into Arabidopsis root vacuolar vesicles. A, K^+ ($^{86}Rb^+$) uptake into vacuolar vesicles. Benzamil (10 μM; arrow) was added 2 min after addition of ^{86}Rb. K^+ concentration was 50 mM. B, Effect of various cation chlorides (300 μM) on K^+ ($^{86}Rb^+$) uptake at 8 min. Values shown are means ± SE from six replicate measurements.

The Arabidopsis *AtCCX3* and *AtsCCX3* were also heterologously expressed in tobacco (KY14 variety). As shown in Figure 8C, *AtCCX3* RNA accumulated in all 35S::*AtCCX3* transgenic lines. The inability to detect transcript in the vector lines indicates the specificity of the primers used during the amplification process. Visible alterations in plant growth were readily apparent in the 35S::*AtCCX3*-expressing lines (Fig. 8C). After 3 weeks of growth in sterile conditions, 100% (17 of 17) of the primary transformants expressing 35S::*AtCCX3* formed leaves with small yellowing necrotic lesions (Fig. 8A). After being transferred to soil, the lines appeared to partially recover for a period of 3 to 5 d. After 1 week, these phenotypes reoccurred in all 17 of the primary transformants; however, the roots of these plants did not show altered growth. As shown in Figure 8, A and B, after 3 months, all of the 35S::*AtCCX3*-expressing plants were severely stunted. The 35S::*AtCCX3* transgenic lines with the least dramatic growth changes always displayed low levels of 35S::*AtCCX3* expression (data not shown). In contrast to these dramatic phenotypes, the 12 35S::*AtsCCX3*-expressing lines displayed phenotypes indistinguishable from the vector-expressing controls. Because the 35S::*AtCCX3* phenotypes were so dramatic, we repeated the transformation process and obtained identical results in a replicate experiment (data not shown).

35S::*AtCCX3* lines were selected for further study on the basis of their T1 phenotype and their ability to make seeds. All lines analyzed that displayed the altered morphology were fertile (n = 13). The same growth abnormalities revisited all of the lines in the second generation. When grown from seed in tissue culture, the T2 plants appeared normal and unperturbed for the first 2 weeks, after which time the leaves began to display altered growth phenotypes (data not shown). T2 35S::*AtCCX3*-transformed plants that were sown and grown in the greenhouse also displayed leaf symptoms after 3 weeks of growth (Fig. 8B). Once again, none of the 35S::*AtsCCX3*- or vector control-expressing plants displayed these phenotypes.

Effects of *AtCCX3* on Plant Growth

The symptoms of the 35S::*AtCCX3*-expressing tobacco plants could not be phenocopied in vector control lines under any growth conditions tested (excess and depleted Na^+, Mg^{2+}, K^+, Mn^{2+}, and Ca^{2+}; data not shown). Primary transformants and T2 35S::*AtCCX3*-expressing plants displayed altered morphology regardless of the medium used for growth. Con-

Downloaded from on January 17, 2018 - Published by www.plantphysiol.org
Copyright © 2008 American Society of Plant Biologists. All rights reserved.

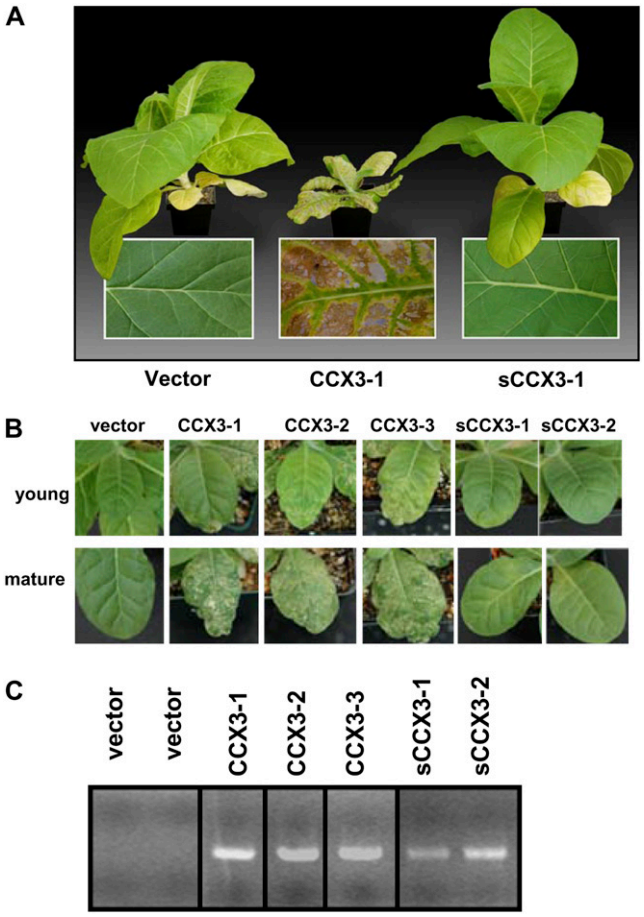

Figure 8. Ectopic expression of *AtCCX3* in tobacco. A, Phenotypes of tobacco plants expressing vector, *AtCCX3*, or truncated *AtCCX3* (AtsCCX3). Only *AtCCX3*-expressing lines displayed stunted growth, yellowing of the leaves, and necrosis of the leaf interveinal tissue. B, *AtCCX3*-expressing tobacco plants displayed yellow lesions at the tips in young leaves, and this became more apparent as the leaves aged (mature). These growth abnormalities were never seen in control lines regardless of age. C, *AtCCX3* expression in the tobacco transgenic lines. Total RNA was isolated from 4-week-old leaf tissue, and 5 μg of RNA was used in the RT-PCR.

ceivably, constitutive *AtCCX3* expression may alter various mineral levels simultaneously, making suppression of the phenotypes dependent on the addition or subtraction of multiple components. To ascertain whether 35S::*AtCCX3* expression altered ion content, we measured the total accumulation of ions in both mature and young leaves. In 35S::*AtCCX3*-expressing plants, young leaves accumulated at least 40% more K^+ and Na^+ (Fig. 9A) compared with control lines and maintained these increased levels for K^+ and Na^+, even as the leaves matured (Fig. 9B). Mn^{2+} levels also increased as the plant leaves matured. One explanation for these growth defects is that the alterations in cellular Mn^{2+} and other cations may produce excess reactive oxygen species. To test this, we isolated total leaf protein from vector- and 35S::*AtCCX3*-expressing plants and detected the carbonyl content of the proteins. As shown in Supplemental Figure S3A, the protein carbonyl content was higher in 35S::*AtCCX3*-expressing plants compared with vector controls and *Ats*CCX3-expressing lines. In fact, these alterations were detectable before the onset of morphological changes in leaf architecture. Together, these findings suggest that *AtCCX3* has a role in ion homeostasis in plants and that when *AtCCX3* expression is heightened, increases in protein oxidation occur.

DISCUSSION

The plant vacuole is a cation depot, and numerous transporters have been proposed to mediate influx and efflux from this endomembrane compartment (Marty,

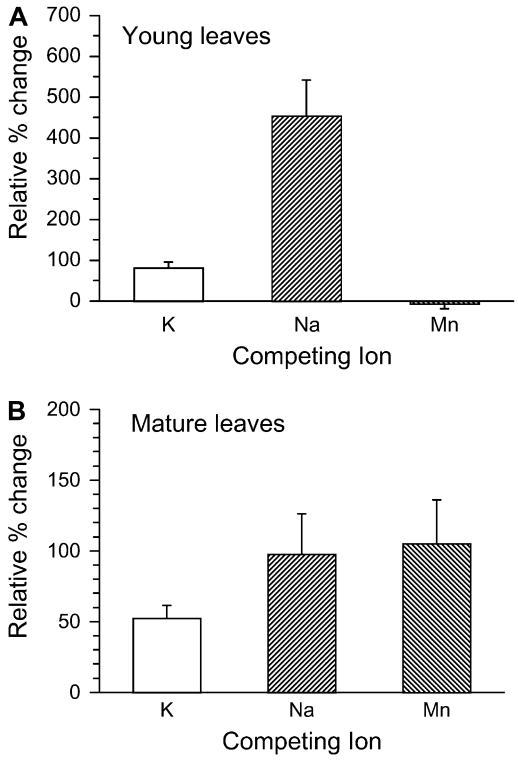

Figure 9. Cation content in young and mature leaves of *AtCCX3*-expressing tobacco plants. ICP analysis from tobacco plants expressing *AtCCX3*. Relative percentage differences in the averages of seven independent lines are shown in the graphs. A, ICP analysis of young leaves from 28-d-old tobacco plants. B, ICP analysis of mature leaves from 40-d-old tobacco plants. SE is for the relative percentage difference of the means. SE was calculated as (mean CCX3/mean vector) × [square root [((SE CCX3)^2/(mean CCX3)^2) + ((SE vector)^2/(mean vector)^2)]] × 100 (http://www.census.gov/acs/www/Downloads/ACS/PercChg.pdf). Concentrations of K^+, Na^+, and Mn^{2+} ions in young leaves were 41,852, 2,150, and 170 μg g^{-1} for plants expressing vector compared with 75,800, 11,904, and 158 μg g^{-1} for plants expressing 35S::*AtCCX3*. Concentrations of K^+, Na^+, and Mn^{2+} ions in mature leaves was 50,644, 3,127, and 98 μg g^{-1} for plants expressing vector compared with 77,051, 6,181, and 201 μg g^{-1} for plants expressing 35S::*AtCCX3*.

Downloaded from on January 17, 2018 - Published by www.plantphysiol.org
Copyright © 2008 American Society of Plant Biologists. All rights reserved.

1999; Maeshima, 2000; Ratajczak, 2000; Hirschi, 2001). Here, we use yeast suppression screens, in planta expression analysis, yeast and plant membrane transport studies, and AtCCX-generated phenotypes in transgenic tobacco to suggest that *AtCCX3* expression is judiciously regulated and is part of an ensemble of transporters regulating K^+, Na^+, and possibly Mn^{2+} levels within plant cells.

Sequence Comparison of *AtCCX*s and *HsNCKX6*

Phylogenetic analysis recently identified five Arabidopsis CCX transporters as being closely related to mammalian K^+-dependent Na^+/Ca^{2+} exchangers (Supplemental Fig. S1A; Shigaki et al., 2006). The functions of AtCCX1 to AtCCX5 in plants are unknown, although they may functionally resemble NCKXs. NCKX exchangers are involved in mammalian signaling (Blaustein and Lederer, 1999; Lee et al., 2002) by catalyzing the electrogenic countertransport of four Na^+ for one Ca^{2+} and one K^+ (Cervetto et al., 1989; Dong et al., 2001). Like the HsNCKX6, AtCCX3 and AtCCX4 have similar conserved α-repeats (Supplemental Fig. S1B), which may play a critical role in maintaining a proper chemical microenvironment for ion binding (Cai and Lytton, 2004b). AtCCX3, AtCCX4, and HsNCKX6 also share similar membrane topologies, which differ from that of AtCAX1 (Supplemental Fig. S1C).

Function of *AtCCX3* and *AtCCX4* in Yeast

Our data show that AtCCX3 and AtCCX4 have functions distinct from AtNHX1. Results from transport assays in yeast are consistent with the phylogenetic analysis and indicate a possible Na^+/K^+ transport function for AtCCX3 and AtCCX4 (Fig. 1; Shigaki et al., 2006). Like *AtNHX1*, *AtCCX3*- and *AtCCX4*-expressing cells can suppress the Na^+ and K^+ sensitivities of mutant yeast strains defective in vacuolar Na^+ and K^+ transport (Fig. 1, B and C). Similarly, AtCCX3-mediated K^+ ($^{86}Rb^+$) uptake in yeast cells was similar to that of *AtNHX1*-expressing cells (Fig. 2). However, benzamil had greater inhibition of $^{86}Rb^+$ uptake in cells expressing *AtNHX1* than in cells expressing *AtCCX3*. Furthermore, *AtCCX3*-expressing yeast cells facilitated the uptake of various cations at concentrations comparable to that of *AtNHX1*-expressing cells (Fig. 3). These results support the idea that AtCCX3 activity promotes K^+ and Na^+ accumulation into endomembrane compartments such as the vacuole.

AtCCX3- and *AtCCX4*-expressing yeast cells did not completely phenocopy *AtNHX1*-expressing yeast cells. *AtCCX3*- and *AtCCX4*-expressing cells could not suppress the hygromycin sensitivity of *nhx1*-deficient cells (data not shown; Nass and Rao, 1998; Darley et al., 2000). Both AtCCX3 and AtNHX1 are predominantly localized to the vacuole (see below), in contrast to the prevacuolar localization of yeast NHXp1 (Nass and Rao, 1998). A possible altered localization could explain the inability of *AtCCX3*-expressing cells to suppress this defect in the yeast secretory pathway. *AtCCX3* expression suppressed the growth sensitivity in a yeast strain defective in both plasma and vacuolar membrane Mn^{2+} transport (Fig. 1D; Supek et al., 1996; Cohen et al., 2000; Luk and Culotta, 2001). The ability of AtCCX3 to suppress the growth defects of a Mn^{2+}-sensitive yeast strain as well as excess Mn^{2+} decreasing $^{86}Rb^+$ uptake in yeast vacuolar vesicles suggest that AtCCX3 is involved in Mn^{2+} homeostasis. The ability to suppress yeast growth defects in Na^+ and Mn^{2+} homeostasis has not been observed with heterologous expression of AtNHX1 or AtCAX1 and suggests that AtCCX3 has distinct transport properties.

Our other yeast data further support AtCCX3 and AtCCX4 having biochemical functions distinct from CAX transporters. For example, N-terminal truncations of AtCAX1 and AtCAX2 suppress the Ca^{2+} sensitivity of yeast cells defective in vacuolar Ca^{2+} transport (Hirschi et al., 1996). In contrast, expression of both full-length and N-terminal truncations of AtCCX3 and AtCCX4 in yeast could not suppress these Ca^{2+} transport defects. Furthermore, the N-terminal domains of AtCCX3 and AtCCX4 were required for function. The requirement of the N-terminal domain in these yeast assays suggests that AtCCX3 and AtCCX4 do not contain a CAX-like N-terminal regulatory domain.

AtCCX3 Is an Endomembrane-Localized Transporter in Flowers

Functional epitope tags of AtCCX3 demonstrated that AtCCX3 localized to the endomembrane in both yeast and plants (Figs. 4 and 5). Furthermore, AtCCX3 appeared to function at the yeast vacuolar membrane as a cation transporter (Figs. 1 and 2). Whether AtCCX3 is localized exclusively on the plant vacuole or also on the trans-Golgi network and prevacuolar compartment is unclear at this time.

Although the precise role of AtCCX3 is still unclear, low AtCCX3 expression levels suggest that AtCCX3 might have a role in cation uptake in a specific subset of cells rather than be involved in bulk cation uptake (Fig. 6). Furthermore, the localization of AtCCX3 to the plant vacuole, and possibly other endomembrane compartments, combined with expression in floral tissue (Supplemental Fig. S2, A and B; publicly available microarray data) propose possible functions associated with the pollen vacuole during tube elongation and polarized tip growth (Cheung et al., 2003; Holdaway-Clarke et al., 2003).

AtCCX3 Phenotypes in Plants

AtCCX3 and AtCCX4 may function in concert with numerous other transporters to regulate pollen growth. The *atccx3* and *atccx4* lines displayed no altered pollen phenotypes, and general plant growth

Downloaded from on January 17, 2018 - Published by www.plantphysiol.org
Copyright © 2008 American Society of Plant Biologists. All rights reserved.

appeared robust in all our assays (Supplemental Fig. S2, B and C; data not shown). This lack of altered growth could be related to the expression of other AtCCX transporters during vegetative and pollen development (Sze et al., 2004; Bock et al., 2006). Many Arabidopsis T-DNA mutants lack any morphological phenotype, presumably due to functional redundancy (Krysan et al., 1999). Our working hypothesis is that AtCCX3 and AtCCX4 have similar functions because they arose from a gene duplication.

The strong phenotype resulting from overexpression of *AtCCX3* in tobacco indicates that *AtCCX3* must be carefully modulated. Tobacco plants ectopically expressing 35S::*AtCCX3* were stunted in growth and contained necrotic lesions in the leaf interveinal regions (Fig. 8A). These tobacco phenotypes differentiate *AtCCX3* from both *AtCAX1*- and *AtNHX1*-overexpressing phenotypes. The *AtCCX3* phenotypes were not observed in plants expressing *AtsCCX3* (Fig. 8A). In contrast, ectopic expression of *AtsCAX1* in tobacco produces dramatic phenotypes (Hirschi, 1999). This further suggests that AtCCX3 does not contain an N-terminal regulatory domain. The fundamental cause of *AtCCX3*-mediated tobacco phenotypes is less apparent than with the *AtsCAX1*-expressing lines. That is, *AtsCAX1*-expressing lines are Ca^{2+} deficient and application of exogenous Ca^{2+} can restore normal growth (Hirschi, 1999). In contrast, the *AtCCX3*-expressing lines could not be rescued by enhancing or reducing NaCl, KCl, or $MnCl_2$ levels (data not shown). Possibly, the *AtCCX3*-expressing lines disrupt tonoplast V-type H^+-translocating ATPase activity, causing a general disruption in pH homeostasis. In fact, altered expression of CAX transporters can produce alterations in vacuolar H^+-ATPase activity (Shigaki and Hirschi, 2006); however, these CAX phenotypes are not as severe at those documented here. Like *AtNHX1*-expressing plants, *AtCCX3* lines were able to accumulate Na^+; however, unlike *AtNHX1*-expressing lines, these plants did not appear to be Na^+ tolerant (data not shown; Apse et al., 1999, 2003).

Although no phenotypes related to changes in Mn^{2+} concentrations could be observed in Arabidopsis either lacking or expressing 35S::*AtCCX3*, the Mn^{2+} inhibition of ^{86}Rb uptake in vacuole-enriched vesicles suggests that AtCCX3 has a role in Mn^{2+} homeostasis (Fig. 7B). This lack of whole plant phenotypes could be related to functional redundancy that may prohibit fluctuations in Mn^{2+} content that could cause deleterious phenotypes in Arabidopsis (Pittman et al., 2004a).

Protein Oxidation Is Increased in Plants Expressing *AtCCX3*

AtCCX3 function may be related to plant reactive oxygen species signaling (Supplemental Fig. S3). Indeed, tobacco plants expressing 35S::*AtCCX3* showed much higher oxidation of proteins compared with controls (Supplemental Fig. S3). The drastic phenotypes observed in 35S::*AtCCX3* tobacco lines may be due to the perturbation of transient metal concentrations in *AtCCX3*-expressing tobacco lines (Figs. 8 and 9). Regulation of metal concentrations is essential for plant antioxidant systems (Halliwell and Gutteridge, 2006). When in excess, these metals can produce highly toxic hydroxyl radicals through a Fenton reaction, resulting in oxidative damage (Halliwell, 2006).

In summary, we have characterized what are to our knowledge the first CCX transporters from plants. We demonstrate that AtCCX3 resides predominantly on an endomembrane and may function as an H^+-dependent K^+ transporter that can also transport Na^+ and Mn^{2+}. The ability to transport both monovalent and divalent cations will need to be directly demonstrated, although it is analogous to yeast SMF1, which transports Fe^{2+} and is permeable by Na^+, Li^+, and K^+ (Chen et al., 1999). This dual-capacity transport suggests a role in vacuolar cation homeostasis in planta, which might protect a subset of cells from metal ion overload (Chen et al., 1999).

MATERIALS AND METHODS

See Supplemental Table S1 for primer information.

Cloning of AtCCX3 and AtCCX4 cDNAs and Plasmid DNA Constructs

AtCCX3 and *AtCCX4* were amplified from Arabidopsis (*Arabidopsis thaliana*) genomic DNA using PCR. Both AtCCX3 and AtCCX4 are predicted to have no introns. The primers are listed in Supplemental Table S1 (primers 1–5).

AtCCX3, AtsCCX3, and *AtCCX4* cDNAs were subcloned into the yeast expression vector piHGpd (Nathan et al., 1999; Pittman and Hirschi, 2001; Pittman et al., 2002a).

The AtsCAX2 plasmid was cloned previously (Shigaki et al., 2003). The Arabidopsis Na^+/H^+ exchanger *AtNHX1* was PCR cloned from plasmid DNA with the primers listed in Supplemental Table S1 (primers 6 and 7) and cloned into yeast expression vectors.

The *AtCCX3* and AtsCCX3 ORFs were cloned into a modified pBIN19 vector (Dr. Toshiro Shigaki, Clontech, personal communication). The resulting constructs contained the cauliflower mosaic virus 35S promoter fragment driving expression of the transporters and the NOS terminator (Hull et al., 2000).

The triple HA epitope-tagged *AtCCX3* (HA-*AtCCX3*) was constructed as described previously (Shigaki et al., 2001). The primers used are listed in Supplemental Table S1 (primers 8–11). The two fragments were ligated with the yeast expression vector piHGpd (Nathan et al., 1999).

The C-terminal GFP tag *AtCCX3* (CCX3-GFP) was constructed as described previously (Cheng et al., 2004). The primers used are listed in Supplemental Table S1 (primers 12–15). After cloning into the appropriate yeast vectors, this expression cassette was also cloned into pBIN19.

Yeast Strains and Growth Conditions

The following *Saccharomyces cerevisiae* yeast strains were used in this study: W303-1A (*MATa* ade2-1 can1-100 his3-11,15 leu2-3, 112 trp1-1 ura3-1; Wallis et al., 1989) and R100 (Δnhx1::URA3; Nass et al., 1997), which is isogenic to W303 and AXT3 (*ena1*::HIS3::*ena4*, *nha1*::LEU2, *nhx1*::TRP1, *ura3-1*; Yokoi et al., 2002). The Mn^{2+}-sensitive strain Δsmf1 + Δsmf2 was used in yeast growth assays (Cohen et al., 2000). The Mg^{2+}-sensitive yeast strain CM66 (*MATa* Δalr1::HIS3, Δalr2::TRP, his3-v200, ura3-52, leu2-v1, lys2-v202 trp1-v63; Liu et al., 2002) was used in yeast growth assays as well. The yeast strains K661 (*MATa* Δvcx1::URA3, ade2-1 can1-100 his3-11,15 leu2-3,112 trp1-1 ura3-1; Cunningham and Fink, 1996) and K667 (cnb1::LEU2 pmc1::TRP1 vcx1Δ; Cunningham and Fink, 1996) were also used in yeast growth assays. Yeast

Downloaded from on January 17, 2018 - Published by www.plantphysiol.org
Copyright © 2008 American Society of Plant Biologists. All rights reserved.

metal-sensitive growth assays were performed as described previously (Hirschi et al., 1996; Nass et al., 1997; Nass and Rao, 1998; Darley et al., 2000; Shigaki et al., 2003; Padmanaban et al., 2007). Yeast samples for liquid culture assays were 5-fold serial diluted, and 10 μL of the 125-fold diluted inoculum was grown in 190 μL of medium supplemented with various concentrations of $NaCl_2$, KCl, and $MnCl_2$ at 30°C with continuous shaking. For the $NaCl_2$ assays in the AXT3 strain, the medium was supplemented with 1 mM KCl (Yokoi et al., 2002). After 48 h, optical density at 600 nm (OD_{600}) measurements were taken.

Yeast Sample Processing and Cation Analysis

Yeast culture conditions and sample processing were modified from previous studies (Lahner et al., 2003; Eide et al., 2005; Mei et al., 2007). Yeast strains expressing vector, *AtNHX1*, or *AtCCX3* were grown overnight in AP medium. After measuring the OD_{600}, equal numbers of cells were grown in 5 mL of yeast peptone dextrose (YPD) supplemented with 100 mM NaCl or 200 μM $MnCl_2$ for 16 h.

Plant Materials and Growth

Arabidopsis ecotype Columbia was used as the wild type. *Agrobacterium tumefaciens* GV3101 was transformed with *AtCCX3*, AtsCCX3, or vector controls (Sambrook et al., 1989). Arabidopsis plants were transformed using the floral dip method (Clough and Bent, 1998). Tobacco (*Nicotiana tabacum* 'KY14'; Koren'kov et al., 2007) transformation was done using the leaf disc method as described previously (Tarczynski et al., 1992).

Cation Analysis of Tobacco and Arabidopsis Plants

Arabidopsis seeds expressing 35S:AtCCX3 were planted on half-strength Murashige and Skoog (MS) + 1% Suc plates and grown for 10 d. Plants were transferred to soil and watered with 100 mL of 50 mM NaCl twice weekly. Plants were harvested at 35 d of age, dried at 68°C, and ground. Tobacco seeds were germinated on half-strength MS + 3% Suc and grown for 2 weeks, then they were transferred to soil. At 28 and 40 d of age, leaves were removed, dried at 68°C, and ground. Inductively coupled plasma (ICP) analysis was done as described previously (Franson, 1989).

$^{86}Rb^+$ Uptake Assay in Yeast and Arabidopsis Roots

A yeast strain (wx1) expressing *AtCCX3*, *AtNHX1*, and vector were grown for 16 h in AP selection medium, and membrane vesicles were isolated as described previously (Pittman and Hirschi, 2001; Cheng and Hirschi, 2003; Pittman et al., 2004b). Plants were grown hydroponically, and membrane vesicles were isolated as described previously (Pittman and Hirschi, 2001; Shigaki et al., 2001, 2003; Cheng et al., 2003).

Time-dependent $^{86}Rb^+$ uptake measurements into membrane vesicles were performed as described previously (Venema et al., 2002; Cheng et al., 2003; Pittman et al., 2004a, 2004b). For the measurement of ΔpH-dependent KCl uptake, vacuole-enriched membrane (100 μg protein mL^{-1}) vesicles were incubated in buffer containing 0.3 M sorbitol, 5 mM Tris-MES (pH 7.6), 25 mM KCl, 0.1 mM sodium azide, and 0.2 mM sodium orthovanadate. The vesicles were added to 1 mM $MgSO_4$ and 1 mM ATP to reach a steady-state pH gradient for 5 min at 25°C before the addition of $^{86}Rb^+$ (1 μCi mL^{-1}; GE Bioscience). Benzamil was used at 10 μM to inhibit AtNHX1 uptake. For metal competition experiments, 25 μM $^{86}Rb^+$ uptake was measured at the 8-min time point in the presence of 300 μM concentrations of the nonradioactive metals KCl, NaCl, $CaCl_2$, $MnCl_2$, and $ZnCl_2$.

Protein Isolation and Western-Blot Analysis of Epitope-Tagged AtCCX3 from Yeast and Plants

Total protein was isolated from yeast expressing HA-*AtCCX3* using the glass bead method (Ausubel et al., 1998). Suc fractionation and western blotting of membranes were done as described previously (Pittman et al., 2004a, 2004b). The vacuolar marker ALP (Molecular Probes) was used at a 1:2,000 dilution, and the plasma membrane H^+-ATPase Pma1p was used at a 1:1,000 dilution. For the GFP-tagged protein, total plant protein was isolated as described previously (Fitzpatrick and Keegstra, 2001).

Microsomal membranes were prepared from AtCCX3-GFP-expressing Arabidopsis leaf tissues as described previously (Cheng et al., 2003). Immunoblotting was performed as described previously (Pittman and Hirschi, 2001). The GFP epitope and the membrane marker proteins were detected as described previously (Cheng et al., 2003).

Onion Epidermis Bombardment and Visualization of the GFP Subcellular Localization

Single epidermis layers were removed from white onion (*Allium cepa*) bulb and placed on the surface of a MS plate (Murashige and Skoog, 1962) containing 2% Suc and 50 μg mL^{-1} ampicillin. The constructs 35S::CCX3-GFP and 35S::GFP were introduced into onion epidermal cells by particle bombardment. The process of particle preparation, coating, and bombardment was as described previously (Sivitz et al., 2007). The GFP fluorescence acquisition was performed with a Plan Apo 20×/0.75 numerical aperture objective. Images were recorded with picture size of 512 × 512 pixels. Individual sections along whole cells were captured in IDS format and then transferred into TIFF files.

RNA Extraction and RT-PCR

RNA was isolated using the RNeasy Plant Kit (Qiagen) according to the instructions of the manufacturer. RT-PCR was performed to detect mRNA transcript in Arabidopsis of *AtCCX3* and *AtCCX4* knockout lines, Arabidopsis plants overexpressing *AtCCX3* and AtsCCX3, and tobacco plants ectopically expressing *AtCCX3* and AtsCCX3. One microliter of the first-strand cDNA was used to amplify an *AtCCX3* gene-specific fragment and an *Actin1* fragment (Geisler et al., 2000). Primers are listed in Supplemental Table S1 (primers 18–23). The relative intensities in different lanes within each individual experiment were independent of the number of PCR cycles performed.

Isolation of Homozygous T-DNA Insertional Lines

To isolate *ccx3* and *ccx4* null alleles, two T-DNA insertional lines were obtained from the SAIL T-DNA insertion collection (Sessions et al., 2002) for *AtCCX3* (SAIL_F-09, *ccx3-1*; SAIL_C30-05, *ccx3-2*) and two from the SALK T-DNA insertion collection (Alonso et al., 2003) for *AtCCX4* (SALK_113447, *ccx4-1*; SALK_040272, *ccx4-2*). Homozygous plants from each T3 generation were obtained by PCR screening using primers listed in Supplemental Table S1 (primers 24–27). For *AtCCX4*, primers 5 and 28 listed in Supplemental Table S1 were used.

Quantitative Real-Time PCR Analysis of AtCCX3

At 14 d of age, 25 plants were transferred to control medium or medium supplemented with 100 mM KCl, 50 mM NaCl, or 1 μM $MnCl_2$. After 24 h, the plants were harvested and total plant RNA was extracted using the RNeasy Plant Kit (Qiagen). For floral RNA, 25 plants were transferred to soil and watered weekly with 50 mL of 100 mM KCl, 50 mM NaCl, or 1 μM $MnCl_2$ solution. RNA was extracted using the RNeasy Plant Kit (Qiagen). Serial dilutions of RNA were made from 5 μg to 5 ng, and first-strand cDNA was synthesized as described previously (Geisler et al., 2000). The PCR amplification was performed with 5 μL of cDNA, 0.5 μM of each primer, and 1× SYBR Green PCR mix (Invitrogen). The primers used are listed in Supplemental Table S1 (primers 29–34). Quantitative PCR was done using the SYBR Green probe, 1 μg of cDNA, and the ABI 7900HT RT-PCR system (Applied Biosystems). Real-time PCR amplification was performed and calculations were made with the ABI Prism 7700 sequence detection system (Applied Biosystems). Relative transcript abundance was determined using the comparative $\Delta\Delta C_T$ method with SDS software version 2.2.2 (Applied Biosystems). For a standard control, expression of the *18S* ribosomal subunit was used.

Protein Oxidation Analysis

Carbonyl assays for the analysis of oxidized proteins in plant cells were performed as described previously (Levine et al., 1994; Davletova et al., 2005; Cheng et al., 2006). Total protein was isolated from young and old leaves of 6-week-old tobacco plants ectopically expressing *AtCCX3*, AtsCCX3, and vector only, as described previously (Cheng et al., 2006). The oxidized proteins were detected by protein gel blotting using anti-dinitrophenylhydrazone antibody (Davletova et al., 2005).

Downloaded from on January 17, 2018 - Published by www.plantphysiol.org
Copyright © 2008 American Society of Plant Biologists. All rights reserved.

Sequence data from this article can be found in the GenBank/EMBL data libraries under accession numbers AtCCX3: NM_112262 and AtCCX4: NM_104289.

Supplemental Data

The following materials are available in the online version of this article.

Supplemental Figure S1. AtCCX3 and AtCCX4 amino acid comparison with the CAX family of transporters and HsNCKX6.

Supplemental Figure S2. Altered expression of *AtCCX3* in Arabidopsis mutants.

Supplemental Figure S3. Protein oxidation from tobacco plants expressing *AtCCX3*.

Supplemental Table S1. Oligonucleotide primers used in the experiments.

ACKNOWLEDGMENTS

We thank Dr. Ramon Gonzalez for providing AtNHX1 in pDR196. We thank Bronwyn Barkla and Heven Sze for critical reading of the manuscript. We also thank Adam Gillum for his help with the preparation of the figures.

Received May 8, 2008; accepted August 30, 2008; published September 5, 2008.

LITERATURE CITED

Alonso JM, Stepanova AN, Leisse TJ, Kim CJ, Chen H, Shinn P, Stevenson DK, Zimmerman J, Barajas P, Cheuk R, et al (2003) Genome-wide insertional mutagenesis of Arabidopsis thaliana. Science **301:** 653–657

Apse MP, Aharon GS, Snedden WA, Blumwald E (1999) Salt tolerance conferred by overexpression of a vacuolar Na^+/H^+ antiport in Arabidopsis. Science **285:** 1256–1258

Apse MP, Sottosanto JB, Blumwald E (2003) Vacuolar cation/H^+ exchange, ion homeostasis, and leaf development are altered in a T-DNA insertional mutant of AtNHX1, the Arabidopsis vacuolar Na^+/H^+ antiporter. Plant J **36:** 229–239

Ausubel FM, Brent R, Kingston RE, Moore DD, Seidmena JG, Smith JA, Struhl K (1998) Current Protocols in Molecular Biology. Green Publishing Associates/Wiley International, New York

Barkla BJ, Pantoja O (1996) Physiology of ion transport across the tonoplast of higher plants. Annu Rev Plant Physiol Plant Mol Biol **47:** 159–184

Blaustein MP, Lederer WJ (1999) Sodium/calcium exchange: its physiological implications. Physiol Rev **79:** 763–854

Blumwald E, Poole RJ (1986) Kinetics of $Ca2^+/H^+$ antiport in isolated tonoplast vesicles from storage tissue of *Beta vulgaris* L. Plant Physiol **80:** 727–731

Bock KW, Honys D, Ward JM, Padmanaban S, Nawrocki EP, Hirschi KD, Twell D, Sze H (2006) Integrating membrane transport with male gametophyte development and function through transcriptomics. Plant Physiol **140:** 1151–1168

Cai X, Lytton J (2004a) The cation/Ca^{2+} exchanger superfamily: phylogenetic analysis and structural implications. Mol Biol Evol **21:** 1692–1703

Cai X, Lytton J (2004b) Molecular cloning of a sixth member of the K^+-dependent Na^+/Ca^{2+} exchanger gene family, NCKX6. J Biol Chem **279:** 5867–5876

Carter C, Pan S, Zouhar J, Avila EL, Girke T, Raikhel NV (2004) The vegetative vacuole proteome of *Arabidopsis thaliana* reveals predicted and unexpected proteins. Plant Cell **16:** 3285–3303

Cervetto L, Lagnado L, Perry RJ, Robinson DW, McNaughton PA (1989) Extrusion of calcium from rod outer segments is driven by both sodium and potassium gradients. Nature **337:** 740–743

Chen XZ, Peng JB, Cohen A, Nelson H, Nelson N, Hediger MA (1999) Yeast SMF1 mediates H^+-coupled iron uptake with concomitant uncoupled cation currents. J Biol Chem **274:** 35089–35094

Cheng N, Pittman JK, Shigaki T, Hirschi KD (2002) Characterization of CAX4, an Arabidopsis H^+/cation antiporter. Plant Physiol **128:** 1245–1254

Cheng NH, Hirschi KD (2003) Cloning and characterization of CXIP1, a novel PICOT domain-containing Arabidopsis protein that associates with CAX1. J Biol Chem **278:** 6503–6509

Cheng NH, Liu JZ, Brock A, Nelson RS, Hirschi KD (2006) AtGRXcp, an Arabidopsis chloroplastic glutaredoxin, is critical for protection against protein oxidative damage. J Biol Chem **281:** 26280–26288

Cheng NH, Liu JZ, Nelson RS, Hirschi KD (2004) Characterization of CXIP4, a novel Arabidopsis protein that activates the H^+/Ca^{2+} antiporter, CAX1. FEBS Lett **559:** 99–106

Cheng NH, Pittman JK, Barkla BJ, Shigaki T, Hirschi KD (2003) The *Arabidopsis cax1* mutant exhibits impaired ion homeostasis, development, and hormonal responses and reveals interplay among vacuolar transporters. Plant Cell **15:** 347–364

Cheung AY, Chen CY, Tao LZ, Andreyeva T, Twell D, Wu HM (2003) Regulation of pollen tube growth by Rac-like GTPases. J Exp Bot **54:** 73–81

Clough SJ, Bent AF (1998) Floral dip: a simplified method for Agrobacterium-mediated transformation of Arabidopsis thaliana. Plant J **16:** 735–743

Cohen A, Nelson H, Nelson N (2000) The family of SMF metal ion transporters in yeast cells. J Biol Chem **275:** 33388–33394

Cunningham KW, Fink GR (1996) Calcineurin inhibits VCX1-dependent H^+/Ca^{2+} exchange and induces Ca^{2+} ATPases in Saccharomyces cerevisiae. Mol Cell Biol **16:** 2226–2237

Darley CP, van Wuytswinkel OC, van der Woude K, Mager WH, de Boer AH (2000) Arabidopsis thaliana and Saccharomyces cerevisiae NHX1 genes encode amiloride sensitive electroneutral Na^+/H^+ exchangers. Biochem J **351:** 241–249

Davletova S, Rizhsky L, Liang H, Shengqiang Z, Oliver DJ, Coutu J, Shulaev V, Schlauch K, Mittler R (2005) Cytosolic ascorbate peroxidase 1 is a central component of the reactive oxygen gene network of *Arabidopsis*. Plant Cell **17:** 268–281

Dong H, Light PE, French RJ, Lytton J (2001) Electrophysiological characterization and ionic stoichiometry of the rat brain K^+-dependent Na^+/Ca^{2+} exchanger, NCKX2. J Biol Chem **276:** 25919–25928

Eide D, Clark S, Nair TM, Gehl M, Gribskov M, Guerinot M, Harper J (2005) Characterization of the yeast ionome: a genome-wide analysis of nutrient mineral and trace element homeostasis in Saccharomyces cerevisiae. Genome Biol **6:** R77

Ettinger WF, Clear AM, Fanning KJ, Peck ML (1999) Identification of a Ca^{2+}/H^+ antiport in the plant chloroplast thylakoid membrane. Plant Physiol **119:** 1379–1386

Fitzpatrick LM, Keegstra K (2001) A method for isolating a high yield of Arabidopsis chloroplasts capable of efficient import of precursor proteins. Plant J **27:** 59–65

Franson MAH (1989) 3120 metals by plasma emission spectroscopy. *In* Standard Methods for the Examination of Water and Wastewater. American Public Health Association, Washington, DC, pp 3.53–3.62

Geisler M, Frangne N, Gomes E, Martinoia E, Palmgren MG (2000) The ACA4 gene of Arabidopsis encodes a vacuolar membrane calcium pump that improves salt tolerance in yeast. Plant Physiol **124:** 1814–1827

Gonzalez A, Koren'Kov V, Wagner GJ (1999) A comparison of Zn, Mn, Cd, and Ca transport mechanisms in oat root tonoplast vesicles. Physiol Plant **106:** 203–209

Halliwell B (2006) Reactive species and antioxidants: redox biology is a fundamental theme of aerobic life. Plant Physiol **141:** 312–322

Halliwell B, Gutteridge JMC (2006) Free Radicals in Biology and Medicine, Ed 4. Clarendon Press, Oxford

Hirschi K (2001) Vacuolar H^+/Ca^{2+} transport: who's directing the traffic? Trends Plant Sci **6:** 100–104

Hirschi KD (1999) Expression of *Arabidopsis* CAX1 in tobacco: altered calcium homeostasis and increased stress sensitivity. Plant Cell **11:** 2113–2122

Hirschi KD, Zhen RG, Cunningham KW, Rea PA, Fink GR (1996) CAX1, an H^+/Ca^{2+} antiporter from Arabidopsis. Proc Natl Acad Sci USA **93:** 8782–8786

Holdaway-Clarke TL, Weddle NM, Kim S, Robi A, Parris C, Kunkel JG, Hepler PK (2003) Effect of extracellular calcium, pH and borate on growth oscillations in Lilium formosanum pollen tubes. J Exp Bot **54:** 65–72

Hull AK, Vij R, Celenza JL (2000) Arabidopsis cytochrome P450s that catalyze the first step of tryptophan-dependent indole-3-acetic acid biosynthesis. Proc Natl Acad Sci USA **97:** 2379–2384

Kamiya T, Maeshima M (2004) Residues in internal repeats of the rice cation/H^+ exchanger are involved in the transport and selection of cations. J Biol Chem **279:** 812–819

Kang KJ, Kinjo TG, Szerencsei RT, Schnetkamp PPM (2005) Residues contributing to the Ca^{2+} and K^+ binding pocket of the NCKX2 Na^+/Ca^{2+}-K^+ exchanger. J Biol Chem **280:** 6823–6833

Downloaded from on January 17, 2018 - Published by www.plantphysiol.org
Copyright © 2008 American Society of Plant Biologists. All rights reserved.

Kasai M, Muto S (1990) Ca^{2+} pump and Ca^{2+}/H^+ antiporter in plasma membrane vesicles isolated by aqueous two-phase partitioning from corn leaves. J Membr Biol **114:** 133–142

Koren'kov V, Park S, Cheng NH, Sreevidya C, Lachmansingh J, Morris J, Hirschi K, Wagner G (2007) Enhanced Cd^{2+}-selective root-tonoplast-transport in tobaccos expressing Arabidopsis cation exchangers. Planta **225:** 403–411

Krysan PJ, Young JC, Sussman MR (1999) T-DNA as an insertional mutagen in *Arabidopsis*. Plant Cell **11:** 2283–2290

Lahner B, Gong J, Mahmoudian M, Smith EL, Abid KB, Rogers EE, Guerinot ML, Harper JF, Ward JM, McIntyre L, et al (2003) Genomic scale profiling of nutrient and trace elements in Arabidopsis thaliana. Nat Biotechnol **21:** 1215–1221

Lee SH, Kim MH, Park KH, Earm YE, Ho WK (2002) K^+-dependent Na^+/Ca^{2+} exchange is a major Ca^{2+} clearance mechanism in axon terminals of rat neurohypophysis. J Neurosci **22:** 6891–6899

Levine RL, Williams JA, Stadtman EP, Shacter E, Lester P (1994) Carbonyl assays for determination of oxidatively modified proteins. Methods Enzymol **233:** 346–357

Liu GJ, Martin DK, Gardner RC, Ryan PR (2002) Large Mg^{2+}-dependent currents are associated with the increased expression of ALR1 in Saccharomyces cerevisiae. FEMS Microbiol Lett **213:** 231–237

Liu XF, Supek F, Nelson N, Culotta VC (1997) Negative control of heavy metal uptake by the Saccharomyces cerevisiae BSD2 gene. J Biol Chem **272:** 11763–11769

Luk EEC, Culotta VC (2001) Manganese superoxide dismutase in Saccharomyces cerevisiae acquires its metal co-factor through a pathway involving the Nramp metal transporter, Smf2p. J Biol Chem **276:** 47556–47562

Luo GZ, Wang HW, Huang J, Tian AG, Wang YJ, Zhang JS, Chen SY (2005) A putative plasma membrane cation/proton antiporter from soybean confers salt tolerance in Arabidopsis. Plant Mol Biol **59:** 809–820

Lytton J (2007) Na^+/Ca^{2+} exchangers: three mammalian gene families control Ca^{2+} transport. Biochem J **406:** 365–382

MacDiarmid CW, Gardner RC (1998) Overexpression of the Saccharomyces cerevisiae magnesium transport system confers resistance to aluminum ion. J Biol Chem **273:** 1727–1732

Maeshima M (2000) Vacuolar H^+-pyrophosphatase. Biochim Biophys Acta **1465:** 37–51

Marschner H (1995) Mineral Nutrition of Higher Plants, Ed 2. Academic Press, San Diego

Marty F (1999) Plant vacuoles. Plant Cell **11:** 587–600

Maser P, Thomine S, Schroeder JI, Ward JM, Hirschi K, Sze H, Talke IN, Amtmann A, Maathuis FJM, Sanders D, et al (2001) Phylogenetic relationships within cation transporter families of Arabidopsis. Plant Physiol **126:** 1646–1667

Mei H, Zhao J, Pittman JK, Lachmansingh J, Park S, Hirschi KD (2007) In planta regulation of the Arabidopsis Ca^{2+}/H^+ antiporter CAX1. J Exp Bot **58:** 3419–3427

Murashige T, Skoog F (1962) A revised medium for rapid growth and bioassays with tobacco tissue cultures. Physiol Plant **15:** 473–497

Nass R, Cunningham KW, Rao R (1997) Intracellular sequestration of sodium by a novel Na^+/H^+ exchanger in yeast is enhanced by mutations in the plasma membrane H^+-ATPase: insights into mechanisms of sodium tolerance. J Biol Chem **272:** 26145–26152

Nass R, Rao R (1998) Novel localization of a Na^+/H^+ exchanger in a late endosomal compartment of yeast: implications for vacuole biogenesis. J Biol Chem **273:** 21054–21060

Nathan DF, Vos MH, Lindquist S (1999) Identification of SSF1, CNS1, and HCH1 as multicopy suppressors of a Saccharomyces cerevisiae Hsp90 loss-of-function mutation. Proc Natl Acad Sci USA **96:** 1409–1414

Padmanaban S, Chanroj S, Kwak JM, Li X, Ward JM, Sze H (2007) Participation of endomembrane cation/H^+ exchanger AtCHX20 in osmoregulation of guard cells. Plant Physiol **144:** 82–93

Pardo JM, Serrano R (1989) Structure of a plasma membrane H^+-ATPase gene from the plant Arabidopsis thaliana. J Biol Chem **264:** 8557–8562

Pittman JK, Cheng NH, Shigaki T, Kunta M, Hirschi KD (2004a) Functional dependence on calcineurin by variants of the Saccharomyces cerevisiae vacuolar Ca^{2+}/H^+ exchanger Vcx1p. Mol Microbiol **54:** 1104–1116

Pittman JK, Hirschi KD (2001) Regulation of CAX1, an Arabidopsis Ca^{2+}/H^+ antiporter: identification of an N-terminal autoinhibitory domain. Plant Physiol **127:** 1020–1029

Pittman JK, Shigaki T, Cheng NH, Hirschi KD (2002a) Mechanism of N-terminal autoinhibition in the Arabidopsis Ca^{2+}/H^+ antiporter CAX1. J Biol Chem **277:** 26452–26459

Pittman JK, Shigaki T, Marshall JL, Morris JL, Cheng NH, Hirschi KD (2004b) Functional and regulatory analysis of the Arabidopsis thaliana CAX2 cation transporter. Plant Mol Biol **56:** 959–971

Pittman JK, Sreevidya CS, Shigaki T, Ueoka-Nakanishi H, Hirschi KD (2002b) Distinct N-terminal regulatory domains of Ca^{2+}/H^+ antiporters. Plant Physiol **130:** 1054–1062

Ratajczak R (2000) Structure, function and regulation of the plant vacuolar H^+-translocating ATPase. Biochim Biophys Acta **1465:** 17–36

Salt DE, Wagner GJ (1993) Cadmium transport across tonoplast of vesicles from oat roots: evidence for a Cd^{2+}/H^+ antiport activity. J Biol Chem **268:** 12297–12302

Sambrook J, Fritsch EF, Maniatis T (1989) Molecular Cloning: A Laboratory Manual. Cold Spring Harbor Laboratory Press, Cold Spring Harbor, NY

Schumaker KS, Sze H (1985) A Ca^{2+}/H^+ antiport system driven by the proton electrochemical gradient of a tonoplast H^+-ATPase from oat roots. Plant Physiol **79:** 1111–1117

Sessions A, Burke E, Presting G, Aux G, McElver J, Patton D, Dietrich B, Ho P, Bacwaden J, Ko C, et al (2002) A high-throughput *Arabidopsis* reverse genetics system. Plant Cell **14:** 2985–2994

Shigaki T, Cheng N-h, Pittman JK, Hirschi K (2001) Structural determinants of Ca^{2+} transport in the Arabidopsis H^+/Ca^{2+} antiporter CAX1. J Biol Chem **276:** 43152–43159

Shigaki T, Hirschi KD (2006) Diverse functions and molecular properties emerging for CAX cation/H^+ exchangers in plants. Plant Biol **8:** 419–429

Shigaki T, Pittman JK, Hirschi KD (2003) Manganese specificity determinants in the Arabidopsis metal/H^+ antiporter CAX2. J Biol Chem **278:** 6610–6617

Shigaki T, Rees I, Nakhleh L, Hirschi KD (2006) Identification of three distinct phylogenetic groups of CAX cation/proton antiporters. J Mol Evol **63:** 815–825

Sivitz AB, Reinders A, Johnson ME, Krentz AD, Grof CPL, Perroux JM, Ward JM (2007) Arabidopsis sucrose transporter AtSUC9: high-affinity transport activity, intragenic control of expression, and early flowering mutant phenotype. Plant Physiol **143:** 188–198

Supek F, Supekova L, Nelson H, Nelson N (1996) A yeast manganese transporter related to the macrophage protein involved in conferring resistance to mycobacteria. Proc Natl Acad Sci USA **93:** 5105–5110

Sze H, Padmanaban S, Cellier F, Honys D, Cheng N-H, Bock KW, Conejero G, Li X, Twell D, Ward JM, et al (2004) Expression patterns of a novel AtCHX gene family highlight potential roles in osmotic adjustment and K^+ homeostasis in pollen development. Plant Physiol **136:** 2532–2547

Tarczynski MC, Jensen RG, Bohnert HJ (1992) Expression of a bacterial mtlD gene in transgenic tobacco leads to production and accumulation of mannitol. Proc Natl Acad Sci USA **89:** 2600–2604

Tuttle MS, Radisky D, Li L, Kaplan J (2003) A dominant allele of PDR1 alters transition metal resistance in yeast. J Biol Chem **278:** 1273–1280

Venema K, Belver A, Marin-Manzano MC, Rodriguez-Rosales MP, Donaire JP (2003) A novel intracellular K^+/H^+ antiporter related to Na^+/H^+ antiporters is important for K^+ ion homeostasis in plants. J Biol Chem **278:** 22453–22459

Venema K, Quintero FJ, Pardo JM, Donaire JP (2002) The Arabidopsis Na^+/H^+ exchanger AtNHX1 catalyzes low affinity Na^+ and K^+ transport in reconstituted liposomes. J Biol Chem **277:** 2413–2418

Wallis JW, Chrebet G, Brodsky G, Rolfe M, Rothstein R (1989) A hyper-recombination mutation in S. cerevisiae identifies a novel eukaryotic topoisomerase. Cell **58:** 409–419

Ward JM, Reinders A, Hsu HT, Sze H (1992) Dissociation and reassembly of the vacuolar H^+-ATPase complex from oat roots. Plant Physiol **99:** 161–169

Winkfein RJ, Szerencsei RT, Kinjo TG, Kang KJ, Perizzolo M, Eisner L, Schnetkamp PPM (2003) Scanning mutagenesis of the alpha repeats and of the transmembrane acidic residues of the human retinal cone Na/Ca-K exchanger. Biochemistry **42:** 543–552

Yokoi S, Quintero FJ, Cubero B, Ruiz MT, Bressan RA, Hasegawa PM, Pardo JM (2002) Differential expression and function of Arabidopsis thaliana NHX Na^+/H^+ antiporters in the salt stress response. Plant J **30:** 529–539

Downloaded from on January 17, 2018 - Published by www.plantphysiol.org
Copyright © 2008 American Society of Plant Biologists. All rights reserved.